Dental Materials Journal 2025; : –

Comparative study of the shrinkage behavior of three bulk-fill resin-based composites using the aluminium tooth model with a MOD cavity

Howe SIMPSON[1], Cécile DUVAL[1], Darien DeWOLF[2], Braden SULLIVAN[3], Richard PRICE[3] and Daniel LABRIE[1]

[1] *Department of Physics and Atmospheric Science, Dalhousie University, 6310 Coburg Road, Halifax, Nova Scotia, B3H 4R2, Canada*
[2] *Department of Mathematics and Statistics, St. Francis Xavier University, 4130 University Avenue, Antigonish, Nova Scotia, B2G 2W5, Canada*
[3] *Department of Dental Clinical Sciences, Dalhousie University, 5981 University Avenue, Halifax, Nova Scotia, B3H 4R2, Canada*
Corresponding author, Daniel LABRIE; E-mail: daniel.labrie@dal.ca

This study evaluated the cusp tip deflection of aluminium tooth models with a mesial-occlusal-distal (MOD) cavity filled with three bulk-fill resin-based composites (RBCs), Aura Ultra Universal (Aura), Admira Fusion x-tra Universal (Admira), and Filtek One shade A2 (Filtek One), to assess the level of shrinkage stress they could produce. The models were prepared using a primer, adhesive and a single RBC increment photo-cured for 20 s at a radiance exitance 1.25 W/cm^2. The RBC axial shrinkage strain (ε) and stress (S) were also measured. Micro-computed tomography in combination with silver nitrate infiltration showed no interfacial debonding. The mean cusp tip deflection for Admira was found to be smaller than those for the other two RBCs. Although ε and S for Aura were higher than those for Filtek One, their mean cusp tip deflections were not significantly different. These results could be explained by the temporal behavior of their elastic modulus.

Keywords: Resin composite, Tooth model, Class II cavity, Cusp deflection, Micro-CT

INTRODUCTION

There is abundant evidence demonstrating that polymerization shrinkage induced stress within the restored tooth structure occurs as the resin-based composites (RBCs) polymerize[1-11)]. From *in-vitro* studies, it is known that the degree of cuspal movement is significantly influenced by the size and volume of the cavity, particularly its depth, which in turn affects the compliance of the cavity wall[1,12)]. Due to the absence of marginal ridges, deep mesio-occluso-distal (MOD) cavities are particularly prone to significant cuspal flexure[12)].

An important clinical use of bulk-fill RBCs is the restoration of Class II MOD cavities in premolar and molar teeth[13,14)]. To reduce RBC shrinkage induced stress as the RBC polymerizes, the material properties of RBCs are continually being optimized by the manufacturers[15)]. In particular, novel monomers[16-19)], novel photoinitiators[20-25)], and different filler technologies[26-29)] have been developed to minimize the inherent RBC shrinkage strain[30)] upon curing and the resulting shrinkage-induced stress[8,31)]. Bulk-fill RBCs has been introduced where the increment layer can be twice as thick (up to 4–5 mm) compared to conventional RBCs (1.5–2 mm)[32,33)]. Thus, bulk-fill RBCs can potentially reduce the number of defects in a restoration[34,35)] by reducing the number of increments and hence potentially increase the viability of the restoration.

Many studies[1-7)] have been carried out to measure the deformation of teeth with Class II MOD restorations, comparing different filling and curing techniques and different RBCs. In these studies, the deflection of the cusp tip was used to predict the degree of shrinkage stress along the tooth wall. However, when human teeth were used, there was a large scatter in the cusp tip deflection data, due mainly to the variability in tooth shapes, tooth composition, and cavity dimensions. The large scatter in the human teeth data can be reduced by using nominally identical typodont teeth of epoxy resin that has an elastic modulus comparable to that of dentin[36)]. However, due to the limited spatial resolution of the optical scanner used in this study to determine the deflection of the cusp tips, the experimental error was substantial (up to 3.9 μm as interpreted from the graphs in the publication). This made it challenging to differentiate the deflections induced by different RBCs. As a result, it may be difficult to use human or artificial typodont teeth to evaluate the impact of different types of RBCs on the cusp deflection.

The cusp tip deflection has also been measured using aluminium tooth models[37,38)]. The elastic modulus of aluminium grade 2024-T351 of 72 GPa is comparable to that of dental enamel of approximately 80 GPa[39)]. Most importantly, the variability in results observed with human teeth can be significantly reduced if standardized aluminium tooth models with identical dimensions and identical material properties are used. Regardless of the tooth materials used in these studies, the data in many past studies were collected only for a short duration (10–33 min) after light irradiation, whereas it is well known that the conversion, shrinkage strain and stress can continue to increase hours or even days later[30,31,40-42)]. For example, one study found that the shrinkage stress measured using a tensometer for different RBCs was still increasing 12 h after light exposure[31)]. Furthermore, most previous studies used position sensors that are known to be susceptible to electronic drift and are therefore unsuitable for experiments lasting several hours. To the best of the authors' knowledge, only one

Received Jun 28, 2024: Accepted Nov 27, 2024
doi:10.4012/dmj.2024-191 JOI JST.JSTAGE/dmj/2024-191

study measured the cusp tip deflection of aluminium tooth models up to seven days after light exposure[43] using a micrometer with a resolution of one micron. This study showed a correlation between the cusp tip deflection and the content of addition fragmentation monomers (AFMs)[16] in the RBC. However, the cusp tip deflection data presented had a standard deviation of up to seven microns.

Thus, although the use of cusp deflection to study the consequences of polymerization shrinkage is well established, the authors believe that previous studies have used imprecise experiment designs or equipment. Therefore, this *in vitro* study examined the cusp tip deflections of standardized aluminium tooth models with Class II MOD restorations of three selected bulk-fill RBCs using a stylus-based profilometer. In addition, the axial shrinkage strain and stress given by thin disc specimens were also measured for the three RBCs using established methods to assess the temporal increase of their elastic modulus. The latter property, together with the shrinkage strain, plays a crucial role in the buildup of shrinkage stress in the tooth. The data collected in this study will provide a more fundamental understanding of the shrinkage mechanics of RBCs.

The research null hypotheses are that:

(1) The differences in the mean cusp tip deflection among the groups are not statistically significant, irrespective of the RBC composition, chemistry, stiffness, and time after irradiation.

(2) The differences in the mean shrinkage-induced strain and stress among the groups are not statistically significant, irrespective of the RBC composition, chemistry, stiffness, and time after irradiation.

MATERIALS AND METHODS

Materials

Three commercial bulk-fill RBCs were selected for this study: Aura bulk-fill ultra universal restorative (SDI, Bayswater, Australia), Filtek One bulk-fill restorative A2 shade (3M Oral Care, St. Paul, MN, USA) and Admira fusion x-tra universal shade (VOCO, Cuxhaven, Germany). The RBC compositions, as reported by the manufacturers, together with the abbreviations used in this study, are given in Table 1. Aura is formulated using conventional methacrylate group monomers such as Bis-GMA, TEGDMA, and UDMA. Filtek One uses nanofiller technology and contains two novel addition fragmentation methacrylate monomers designed to partially relieve polymerization stress. Admira is based on a novel organically modified ceramics (ORMOCERs) nanohybrid filler in a resin matrix that contains no conventional monomers. Filtek One was used as the control as this RBC is regularly employed in clinical and material property studies for comparison purposes[44-49].

Aluminium (Al) tooth model and surface preparation

A schematic diagram of the Al tooth model is depicted in Fig. 1. The tooth models were machined using aluminium grade 2024-T351 to an accuracy of 25–50 µm. The Class II MOD cavity had a 4.00 mm depth, 4.00 mm width and

Table 1 Composition of the RBCs and adhesive as provided by the manufacturers

Product (Abbreviation used in this work)	Manufacturer (lot Number)	Resin matrix	Filler	Filler (wt%/vol%)
Aura bulk fill ultra universal restorative (Aura)	SDI (180364, 180541)	UDMA, Bis-EMA, Bis-GMA, TEGDMA	barium alumino-borosilicate glass, silica	81/65
Filtek One bulk fill restorative A2 shade (Filtek One)	3M Oral Care (N942361, N948431, N961097)	proprietary AUDMA and AFM, DDDMA and UDMA	100 nm ytterbium trifluoride, 20 nm silica, 4 to 11 nm zirconia, zirconia/silica cluster filler	76.5/58.4
Admira fusion x-tra universal shade (Admira)	VOCO (1651326, 1711125, 1732094)	MA, ORMOCER, BHT	nanohybrid ORMOCER®, 20–50 nm SiO_2, ~1 µm SiO-based ceramic hybrid fillers	84/69
Scotchbond Universal	3M Oral Care	MDP Phosphate Monomer, Bis-GMA Dimethacrylate, HEMA, Vitrebond™ Copolymer, Ethanol, Water, silane	Nanosilica filler	11/--

proprietary AUDMA: high molecular weight aromatic dimethacrylate, proprietary AFM: addition fragmentation monomers, DDDMA: 1, 12-Dodecanediol dimethacrylate, UDMA: urethane dimethacrylate, MA: Methacrylate, ORMOCER®: Organically Modified Ceramics, BHT: Butylated hydroxytoluene, Bis-EMA: Ethoxylated bis-phenol A dimethacrylate, Bis-GMA: Bisphenol A glycidyl methacrylate, TEGDMA: triethylene glycol dimethacrylate, HEMA: 2-hydroxyethyl methacrylate.

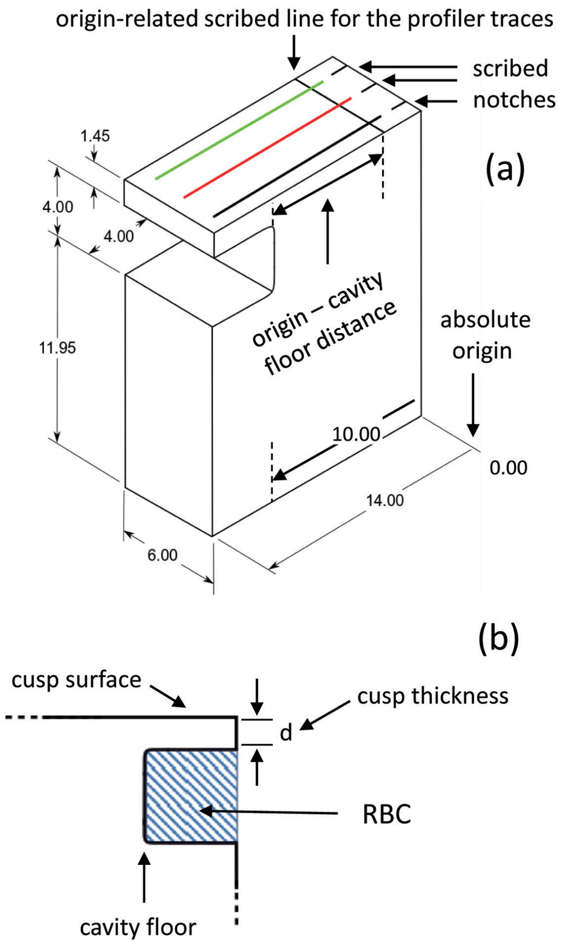

Fig. 1 Schematic diagram of the aluminium tooth model with a 1.45 mm cusp wall thickness.
Note that two walls surrounding the cavity are appreciably thicker than the third cusp wall where most of the deformation occurred. The black, red and green lines indicate the paths taken by the profilometer. The scribed black line across the face of the model serves as the profilometer traces related origin while the three small notches define the trace locations. The origin–cavity floor distance is used to locate the trace origin relative to the floor. Note that the cavity floor and cusp tip are located 10.00 mm and 14.00 mm relative to the absolute origin 0.00 mm, respectively. (b) shows the cavity floor and RBC in the restored tooth model.

6.00 mm length. The inside corners of the MOD cavity had a 1 mm radius equivalent to that generated by a fine diamond round dental bur (no. 8801.31.018, Brasseler Canada, Quebec city, Canada). To limit the deformation produced by the curing RBC around the cavity except along the measured cusp wall, Fig. 1 shows that the thickness of the measured cusp wall was much smaller than the other dimensions of the model. The cavity walls were air abraded using 50 µm particle size 99.6 % aluminium oxide (Korox 50, BEGO, Bremen, Germany).

The external tooth model cusp wall surfaces were polished manually. The tooth model cusp wall surfaces were first sanded using 360, 600, and 1200 SiC paper using water as lubrication. Then, they were polished on a pad (UltraPad™, PSA, 8 in, Buehler, Lake Bluff, IL, USA) using 9 µm size polycrystalline diamond particles in suspension (MetaDi™ Supreme, Poly, 9 µm, Buehler) for 10 min, then on a pad (Trident™, PSA, 8 in, Buehler) using 3 µm size polycrystalline diamond particles in suspension (MetaDi™ Supreme, Poly, 3 µm, Buehler) for 10 min, and finally on a pad (Trident™, PSA, 8 in, Buehler) using 1 µm size polycrystalline diamond particles in suspension (MetaDi™ Supreme, Poly, 1 µm, Buehler) for 15 min. A travelling microscope was used to measure the tooth model's final dimensions to an accuracy better than 100 µm. The tooth models selected for this study had a maximum undulation less than 0.3 µm in the cusp wall surface topography, and the final cusp wall thickness from tooth model to tooth model was between 1.59 and 1.81 mm. Eleven tooth models were selected to be filled with Aura and Filtek One, and ten tooth models were chosen for Admira with a mean cusp wall thickness (standard deviation) of 1.68 (0.06) mm, 1.66 (0.04) mm, and 1.69 (0.08) mm, respectively. Among the three groups of tooth models, the mean cusp wall thickness differed by 1.8%, and the coefficient of variation was less than 4.7%.

Restoration and photo-curing conditions

One layer of primer (Monobond Plus primer, Ivoclar Vivadent, Schaan, Liechtenstein) and three layers of adhesive (Scotchbond™ Universal Adhesive, 3M Oral Care) were applied to the cavity surfaces. Each coat was air dried and photo-cured for 10 s to enhance the bonding between the cavity walls and RBC. Based on a pilot study, this surface preparation was required to obtain high reproducibility in the deflection data along the cusp wall collected on tooth models restored under the same experimental conditions. The adhesive composition, as provided by the manufacturer, is given in Table 1.

Two layers of transparent tape were used to cover the two opposite large open faces of the tooth model, and then the cavity was completely filled with the RBC. A third layer of transparent tape was placed over the remaining open face to confine the RBC within the cavity.

The filled tooth models, RBC samples for the axial shrinkage strain and stress measurements were photocured in the dark at a distance of 0.5–1 mm from the light guide tip using a single emission peak wavelength LED-based light-curing unit (Paradigm Deep Cure LED unit, 3M Oral Care) for 20 s. The light-curing unit (LCU) delivered a radiant power of 800 mW and a radiant exitance of 1.25 W/cm^2 to the specimens. The LCU radiant power at 0.5 mm from the tip was measured using a calibrated thermopile and meter (PM-10 detector and FieldMax meter, Coherent, Santa Clara, CA, USA)[50,51]. Between profilometry measurements, the restored tooth models were stored in the dark and in air at a room temperature of 24±1ºC.

Assessment of interfacial debonding between the primer-adhesive-RBC and Al tooth model walls

Micro-computed tomography (micro-CT), in combination with a radiopaque dye (silver nitrate, $AgNO_3$), was used to assess the interfacial debonding along the restoration margins. The methodology was fully described[52] and is briefly summarized here. The groups consisted of an unrestored Al tooth model with the cavity walls air abraded, but without any surface treatment; two Al tooth models were restored with Aura without, and with primer and without any adhesive, and three Al tooth models were restored with Aura, Filtek One, and Admira with primer and the adhesive. The models were scanned using a micro-CT instrument (XT H 225, Nikon Metrology, Brighton, MI, USA). The scanning parameters were 115 kV acceleration voltage, 100 μA tube current, 720 ms exposure time, 720 projections with 2 frames per projection, and a resolution of 13 μm. After scanning, the restored Al tooth models were stored in a 50 % (w/w) aqueous solution of $AgNO_3$ at room temperature for either 14 h (tooth models with no adhesive) or 48 h (tooth models with adhesive) and then they were re-scanned using the same parameters. Reconstructions were performed using CT Pro 3.1.11 (Nikon metrology) software, and the volumetric analysis was done using VGStudio MAX 3.4 (Volume Graphics, Heidelberg, Germany).

Deflection Measurements at 1 h, 24 h, and 7 days

A novel approach was used to measure the cusp deflection in the restored Al tooth models up to 7 days after light exposure. A stylus-based profilometer (DEKTAK 8, Veeco, Plainview, NY, USA) was employed to measure the surface topography of the tooth model cusp wall lengthwise before restoration and 1 h, 24 h, and 7 days after photo-curing of the restored model. The diameter of the stylus tip was 12.5 μm, and the stylus tracking force was 3 mg. The profilometer data were highly reproducible with a high signal-to-noise ratio. A single trace was recorded in only 30 s. The profilometer data was immune to any long-term electronic or mechanical drift that are present in experimental design that uses position sensors to monitor the cusp deflection at a single point with time. The profilometer trace measurements were collected along the black, red, and green lines centered at the three small notches depicted in Fig. 1. The traces spanned an origin groove scribed across the sample to a target distance near the edge of the sample. The distance from the origin groove to the cavity floor was measured using a travelling microscope. As a result, the trace position relative to the cavity floor was known to within 100 μm. The position axis was translated so that the cavity floor position was set at 10.0 mm in agreement with the diagram shown in Fig. 1. Any small differences in the inclination of the tooth model cusp wall surface relative to the profilometer translation stage were accounted for so that the average sample topography was zero within 2-mm around the origin groove. For this position interval, the deformation of the Al tooth model caused by the restoration was negligible. The net tooth model cusp deflection induced by the photo-cured RBC was given by the difference between the profilometer traces recorded at various times after photo-curing and the traces collected before restoration. The mean cusp tip deflection was obtained by averaging the cusp tip measurement along the three traces on the same restored tooth model while the standard deviation (SD) was calculated using the same three measurements. A typical SD value was only 0.15 μm.

Axial shrinkage strain and stress measurements for 24 h

The axial shrinkage strain and stress were collected continuously for up to 24 h from the start of light exposure. A modified version of the bonded disk method[53,54] was used to measure the axial shrinkage strain where the reflecting top surface of the 100 μm thick glass coverslip placed on top of the RBC sample acted as the "moving mirror" in a Michelson interferometer. The interferometer was temperature stabilised to within 0.001ºC using a temperature controller (Lake Shore Cryotronics, Westerville, OH, USA) to ensure thermal and mechanical stability of the equipment during the experiment. The RBC samples were 1.00 mm thick by 10 mm in diameter, and they were held at T=23ºC. Three replicates were made for each RBC.

A redesigned cantilever-based tensometer was used to collect shrinkage stress data. The tensometer was similar in design to that used previously[31] except that it was made using a single metal (stainless steel 304) to virtually eliminate the effect of the small temperature drift ($\Delta T \leq 0.6$°C) on the stress data. In the new tensometer, the bottom quartz rod was replaced by a 3 mm thick by 25.4 mm diameter quartz disk clamped to the base of the instrument while the top quartz rod was replaced by a 10.00 mm diameter stainless steel rod. The compliance of the tensometer was 0.20 μm/N. The RBC samples tested were 1.00 mm thick and 10.0 mm in diameter. The sample temperature was 24ºC. Three replicates were collected for each RBC.

Statistical analysis

All tests were performed at a pre-set α=0.05.

The cusp tip deflection data was analyzed using a Mixed One-Factor ANOVA with Repeated Measures using SPSS 25.0.0.2. The RBC is the main factor, with each replicate measured at three times (1 h, 24 h, and 7 days). Tukey *post-hoc* pairwise and multiple comparisons were then performed to estimate the differences in the data between different times and between different RBCs. Normality was checked using the Shapiro-Wilk test for normality. The sphericity assumption for this test was checked using Mauchly's test of sphericity. *Post-hoc* power analysis to determine achieved power was computed using G*Power 3.1.9.6[55,56].

The axial shrinkage strain and stress data were analyzed using a Mixed One-Factor ANOVA with Repeated Measures using SPSS 25.0.0.2. The RBC is the main factor, with each replicate measured at two times (1 h and 24 h). Tukey *post-hoc* pairwise and multiple comparisons were then performed to estimate the differences in the data between different times and between different RBCs. Normality was checked using the Shapiro-Wilk test for normality. Homogeneity of variances for each combination of time and RBC was checked using Levene's test for homogeneity of variances. *Post-hoc* power analysis to determine achieved power was computed using G*Power 3.1.9.6[55,56].

RESULTS

Micro-CT imaging

Figures 2 and 3 report the micro-CT examination that looked for interfacial debonding along the margins of five Al tooth models restored with Aura, Filtek One and Admira using different surface treatments to the Al tooth model walls.

Figure 2 displays micro-CT images of the Al tooth models restored using Aura without any surface treatment as the positive control (a) and with primer and no adhesive (b) after storage in silver nitrate. The silver nitrate detected by micro-CT is depicted in red. Figures 2(c) and (d) display the corresponding images (a) and (b), respectively, as high contrast 3D images where the silver nitrate is displayed in yellow and the background in black. Note the leakage of silver nitrate along the walls of the positive control Al tooth model deep into the restoration in Fig. 2(c), while it was detected only along the outer margins of the restoration treated with primer but no adhesive in Fig. 2(d); no silver nitrate was detected along the cavity walls within this restoration.

Figure 3(a) is a micro-CT image of the central part of the Al tooth model. The tooth model walls are clearly defined together with the rounded internal line angles mimicking the round corners of a Class II MOD cavity made by a dental bur. Figures 3(b), (c), and (d) display the regions around the restorations before storage in

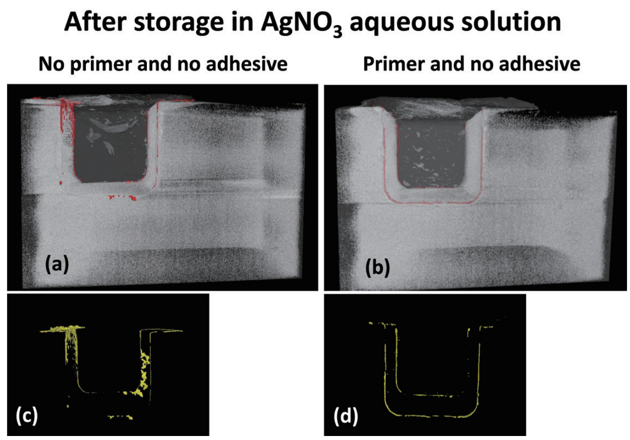

Fig. 2 Micro-CT images of the Al tooth models restored using the Aura without any surface treatment as the positive control (a), and with primer but no adhesive (b) after storage in silver nitrate. The silver nitrate detected by micro-CT is depicted in red. (c) and (d) display the corresponding images (a) and (b), respectively, but using high contrast 3D images where the silver nitrate is displayed in yellow and background in black. Note the leakage of silver nitrate along the walls of the tooth model deep within the restoration in (a) and (c) while it is detected only along the outer margins of the restoration in (b) and (d). The low contrast features within the restorations [(a) and (b)] are attributed to small voids.

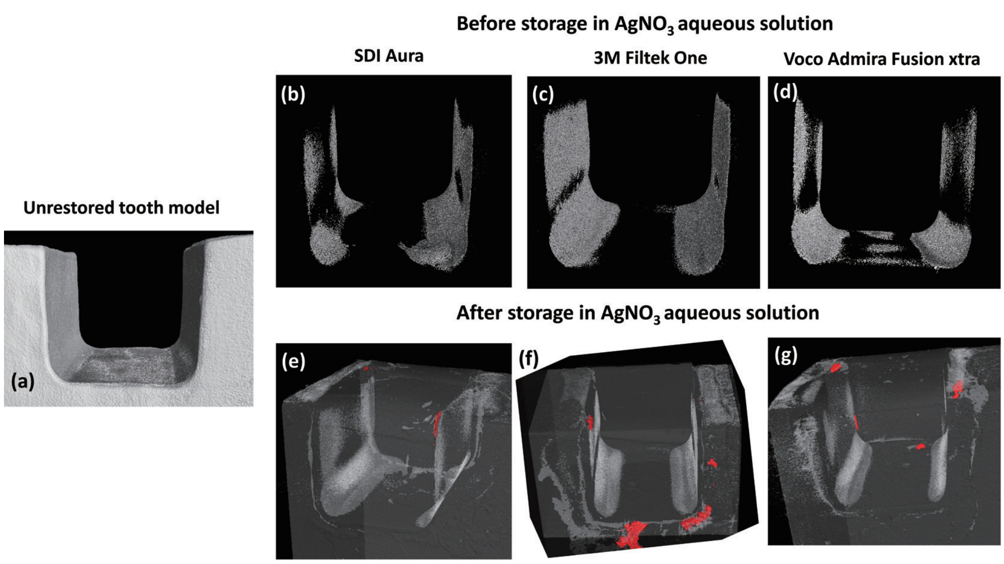

Fig. 3 Micro-CT image of the central part of an unrestored Al tooth model that had not received any surface treatment. (b), (c), and (d) display the regions around the restorations using Aura, Filtek One and Admira with primer and adhesive before storage in silver nitrate. The low-density regions are highlighted. (e), (f), and (g) depict the micro-CT image analysis after storage in silver nitrate solution. Note that for each restoration, the silver nitrate (depicted in red) was detected only at the outer surface of the restored tooth model.

silver nitrate, with the low-density regions highlighted. Note that these regions extend along a large fraction of the cavity walls to the outer edges of the models. Due to the high translucency of the adhesive to X-rays, it is impossible to differentiate between it and any voids or gaps created along the Al tooth model walls. Figures 3(e), (f), and (g) depict the micro-CT image analysis after storage in silver nitrate solution. Due to the high radiopacity of the silver nitrate solution to X-ray, its penetration along any gaps between the RBC and the Al wall can be easily detected. Note that for each restoration, the silver nitrate (depicted in red) was detected only at the outer surface of the restored tooth model. No silver nitrate can be seen along the cavity walls within each restoration. These results show that the highlighted low-density regions observed in Figs. 3(b), (c), and (d) are solely due to the adhesive and that there was no contribution from voids or debonding.

Cusp deflection data

Figure 4 displays the net cusp deflection along the cusp wall for tooth models restored using Aura (a), Admira (b), and Filtek One (c), at 1 h, 24 h, and 7 days after light exposure.

For all three RBCs, most of the cusp deflection occurs within 24 h after light exposure. At seven days after light exposure, the magnitude of the cusp deflections observed in (a), (b), and (c) at a position of 13.4 mm were 13.33 µm, 10.43 µm, and 13.85 µm, respectively.

Figure 5 shows a composite of nine histograms showing the magnitude of the cusp tip deflection at a position of 13.4 mm, measured 1 h (a, d, g), 24 h (b, e, h), and 7 days (c, f, i) after light exposure for the three

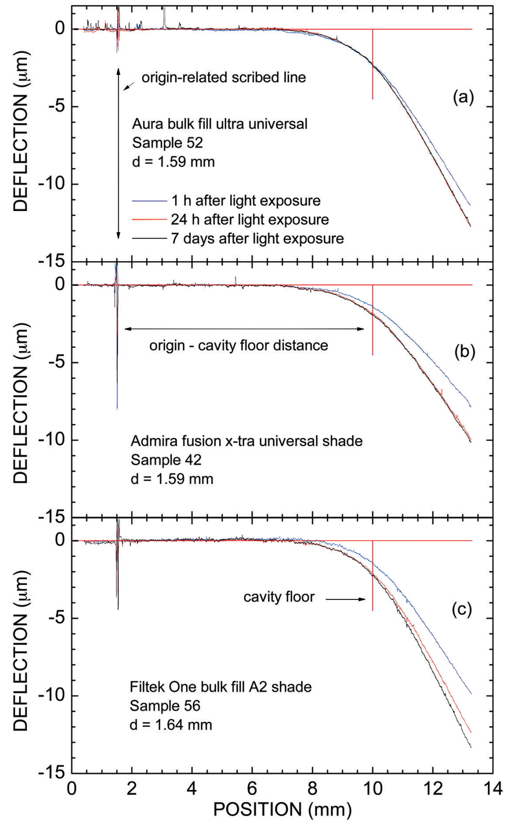

Fig. 4 Cusp deflection in the Al tooth model at 1 h, 24 h, and 7 days after light exposure for; Aura (a), Admira (b), and Filtek One (c).
The vertical lines indicate the position of the cavity floor. Note that most of the cusp deflection occurs within the first 24 h post irradiation.

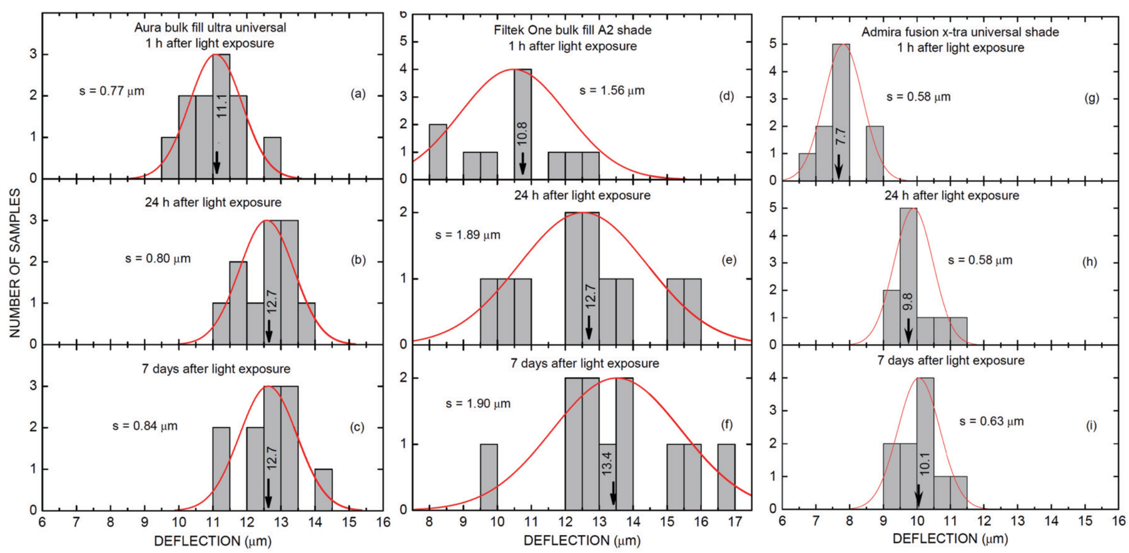

Fig. 5 Histograms of the tooth model cusp tip deflection at the 13.4 mm position measured 1 h (a, d, g), 24 h (b, e, h), and 7 days (c, f, i) after LCU light exposure for the three RBCs examined.
The solid lines were normal distribution functions fitted to the data. The vertical down arrows and numerical values indicate the medians and s stands for the standard deviation. Eleven replicates were used in each of the histograms for the Aura and Filtek One while ten replicates were utilized for the Admira.

RBCs. Eleven replicates each were used to make the histograms for Aura and Filtek One while ten replicates were utilised for the Aura histograms. The cusp tip deflection interval along the x-axis in each histogram is the same. The Shapiro-Wilk test for normality showed that the histograms are normally distributed (all nine *p*-values at least 0.268), as depicted by solid lines fitted to the data in Fig. 5. For each post-irradiation time, the vertical downward arrow indicates the median value, which is close to the mean, and the standard deviation (s). The ANOVA showed that the mean cusp tip deflection differs significantly both between the three RBCs [F(2,29)=22.429, *p*=0.000] and across time [F(2,58)=183.692, *p*=0.000]. There were 32 observations, the result of 11 replicates for each of Aura and Filtek One and ten replicates for Admira, with repeated measures at each of three-time levels. Using a significance level α=0.05, assuming a correlation of 0.7 among repeated measures, and no sphericity correction, the achieved power of this repeated measures ANOVA to detect a medium effect size of 0.25 is 98.35%. Table 2 summarizes comparisons both over time and between composites for mean cusp deflection. The *post-hoc* Tukey intervals show that mean cusp tip deflection for Admira is significantly lower than both Aura and Filtek One. In contrast, mean cusp tip deflection for Aura and Filtek One do not significantly differ. Bonferroni-corrected pairwise comparisons show that mean cusp tip deflection at 1 h is significantly less than at 24 h, and that mean cup tip deflection at 24 h is significantly less than at 7 days. For all three RBCs, the mean cusp tip deflection at 24 h was significantly greater than at 1 h. However, the mean cusp tip deflection at 7 days was significantly greater than that at 24 h only for the Filtek One while there were no significant differences in the mean cusp tip deflection at these two times for the other two RBCs. Mauchly's test of sphericity showed that, for each RBC, there were no significant differences in s between all possible combinations of 1 h, 24 h, and 7 days in each RBC. A wide range in cusp tip deflections was observed for the Filtek One, where at seven days post-irradiation s=1.90 μm while a very narrow distribution was observed for the Admira with s=0.63 μm at the same time. Levene's test for homogeneity of variances confirmed this observation and it detected a significant difference in variances across the three RBCs [L(2,29)=5.023 and *p*=0.013 for 1 h, L(2,29)=4.933 and

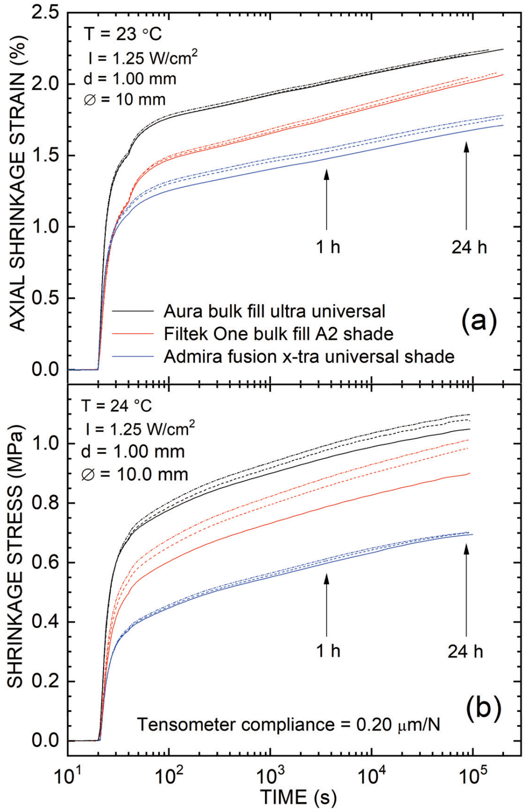

Fig. 6 Axial shrinkage strain (a) and stress (b) as a function of time for the three RBCs examined. The tensometer compliance was 0.20 μm/N. Three replicas were collected for each condition. Note that the relative ordering for the strain and stress data are the same for the three RBCs.

Table 2 Comparisons over time and between composites estimating differences in mean cusp tip deflection

Bonferroni-corrected time comparisons, 95% confidence

Difference	Estimate	Lower bound	Upper bound	*p*-value
24h–1h	1.879	1.548	2.209	0.000
7 days–1h	2.277	1.912	2.642	0.000
7 days–24 h	0.398	0.135	0.661	0.002

Tukey-corrected multiple comparison between composites, 95% confidence

Difference	Estimate	Lower bound	Upper bound	*p*-value
Aura–Admira	2.839	1.624	4.055	0.000
Filtek–Admira	2.914	1.698	4.129	0.000
Filtek–Aura	0.075	−1.111	1.261	0.987

p=0.014 for 24 h, L(2,29)=4.007 and p=0.029 for 7 days]. Based on the Levene's test and the standard deviations calculated from the histograms displayed in Fig. 5, s(Filtek One) is significantly larger than s(Aura) and s(Admira). In addition, it would appear that s(Aura) is not significantly different than s(Admira).

Axial shrinkage strain and stress data

Figure 6 displays the axial shrinkage strain (a) and stress (b) as a function of time up to 24 h post-irradiation for the three RBCs used in this study. Note the same relative ordering for the axial strain (ε) and stress (S) for the three RBCs where the lowest ε and S values were obtained for the Admira. The Shapiro-Wilks test for normality was applied to the six distributions of strain and stress, showing that normal distribution functions can describe them. Levene's test for homogeneity of Variances showed that we can assume equal variance across the three RBCs for both strain and stress, except for the shrinkage stress at 24 h [L(2,6)=5.480, p=0.044]. Given the small number of degrees of freedom, this small violation was ignored in this case, and the assumption of homogeneity was made. The ANOVA with repeated measure models showed that both mean axial shrinkage strain and stress differ significantly over both RBC type [F(2,6)=316.331 and p=0.000 for strain, F(2,6)=85.540 and p=0.000 for stress] and time [F(1,6)=86,715.372 and p=0.000 for strain, F(1,6)=2292.347 and p=0.000 for stress]. Table 3 summarizes comparisons both over time and between composites for mean axial shrinkage strain. Bonferroni-corrected pairwise comparisons show a significant increase in mean axial shrinkage strain from 1 h to 24 h. Tukey *post-hoc* comparisons show that the mean axial shrinkage strain for Aura is significantly larger than Filtek One, and for Filtek One is significantly larger than Admira. Table 4 summarizes comparisons both over time and between composites for mean axial shrinkage stress. Bonferroni-corrected pairwise comparisons also show a significant increase in mean shrinkage stress from 1 h to 24 h. Tukey *post-hoc* comparisons show that mean shrinkage stress for Aura is significantly larger than Filtek One, and for Filtek One is significantly larger than Admira. There were 9 selected observations out of a series of observations covering a time span of 24 h, the result of 3 replicates for each of the three RBCs, with repeated measures at each of two-time levels. Using a significance level α=0.05, assuming a correlation of 0.7 among repeated measures, and no sphericity correction, the achieved power of this repeated measures ANOVA to detect a medium effect size of 0.25 is 37.1%.

To better illustrate the time evolution of the shrinkage-induced strain and stress, Fig. 7 depicts, for each RBC, the average value for each group of three repeats of the strain (a) and stress (b) at selected times normalized to the mean values at 24 h. The standard deviations were less than or equal to the symbol size. The vertical dashed lines are located at 5 min, a time at

Table 3 Comparisons over time and between composites estimating differences in mean shrinkage-induced strain

Bonferroni-corrected time comparison, 95% confidence

Difference	Estimate	Lower bound	Upper bound	p-value
24h–1h	0.215	0.213	0.216	0.000

Tukey-corrected multiple comparison between composites, 95% confidence

Difference	Estimate	Lower bound	Upper bound	p-value
Aura–Admira	0.495	0.434	0.555	0.000
Aura–Filtek	0.213	0.152	0.273	0.000
Filtek–Admira	0.282	0.221	0.343	0.000

Table 4 Comparisons over time and between composites estimating differences in mean shrinkage-induced stress

Bonferroni-corrected time comparison, 95% confidence

Difference	Estimate	Lower bound	Upper bound	p-value
24h–1h	0.104	0.099	0.109	0.000

Tukey-corrected multiple comparison between composites, 95% confidence

Difference	Estimate	Lower bound	Upper bound	p-value
Aura–Admira	0.375	0.285	0.464	0.000
Aura–Filtek	0.128	0.038	0.217	0.011
Filtek–Admira	0.247	0.158	0.336	0.000

which the data from several past studies are cited. The horizontal dashed lines located at 90% of the maximum strain and stress show the time values for which the strain and stress reach 90% of their maximum values.

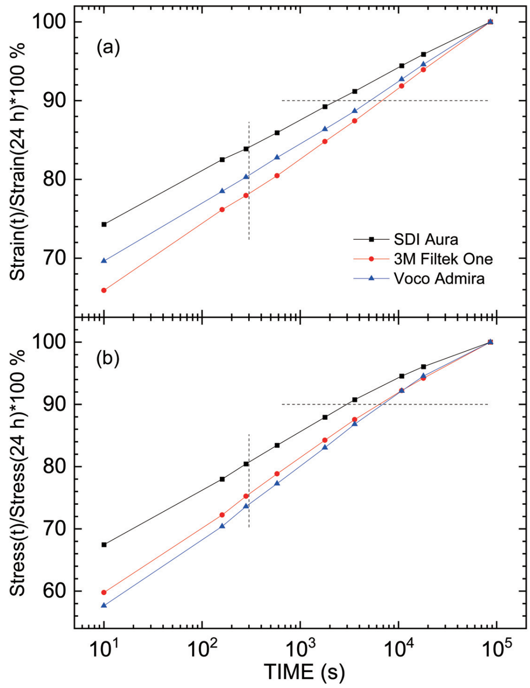

Fig. 7 Mean value of the strain (a) and stress (b) at selected times normalized to the mean values at 24 h for the three RBCs examined.
The mean values were calculated from the three repeats within each group obtained from the data shown in Fig. 6. The standard deviations were less than or equal to the symbol size.

For the three RBCs investigated, at a time of 5 min, the strain reached values between 78% and 84% of their values at 24 h, while the stress values ranged between 74% and 80% of their values at 24 h. On the other hand, the time required to reach 90% of their values at 24 h varied between 40 min and 113 min for the strain and, between 51 min and 118 min for the stress.

As displayed in Fig. 7, the time evolution of the shrinkage stress lags behind that of the shrinkage strain for each RBC. To better illustrate the different time evolution of these two quantities, Fig. 8 depicts the ratio of the normalized stress over the normalized strain

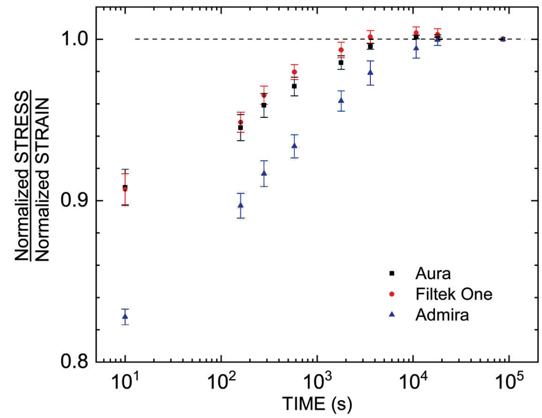

Fig. 8 Ratio of the normalized shrinkage stress over normalized shrinkage strain at selected times up to 24 h after light exposure.
The horizontal dashed line corresponds to the case when the stress and strain have the same time development. Note that the time delay for the Admira is significantly greater than those for the Aura and Filtek One.

Table 5 Mean (standard deviation) for the cup tip deflection (D) at the 13.4 mm position at 1 h, 24 h, and 7 days after light exposure, and axial shrinkage strain (ε) and stress (S) at 1 h and 24 h, after light exposure for the three RBCs investigated in this work

RBC/Data	Aura bulk fill ultra universal	Filtek One bulk fill A2 shade	Admira fusion x-tra universal
D (μm) 1 h	11.08 (0.77)	10.47 (1.56)	7.81 (0.58)
D (μm) 24 h	12.58 (0.80)	12.53 (1.89)	9.90 (0.58)
D (μm) 7 days	12.63 (0.84)	13.52 (1.90)	10.06 (0.63)
Axial e (%) 1 h	2.011 (0.009)	1.77 (0.02)	1.52 (0.04)
Axial e (%) 24 h	2.206 (0.009)	2.02 (0.02)	1.71 (0.04)
S (MPa) 1 h	0.98 (0.03)	0.84 (0.05)	0.608 (0.009)
S (MPa) 24 h	1.08 (0.03)	0.96 (0.06)	0.699 (0.006)
E (GPa)	8.7 (0.2)	11.3 (0.3)	10.1 (0.1)

The flexural modulus (E) as provided by the manufacturers is also reported. The irradiance incident on the sample surface was 1.25 W/cm^2. For the axial ε and S the sample dimensions were 1.00 mm thick by 10 mm diameter. The tensometer compliance was 0.20 μm/N.

at selected times up to 24 h after light exposure. Such a ratio from a direct comparison between the time evolution of the shrinkage strain and stress data is meaningful and informative on the time evolution of the stiffness because the RBC sample dimensions and configuration factors (of 5), sample temperatures, and photocuring conditions were approximately the same between the strain and stress measurements. The horizontal dashed line indicates the case when the time evolution of the stress is the same as the strain. Note that the time lag between the stress and strain is comparable for Aura and Filtek One while it is much larger for Admira.

Table 5 reports the mean values of the cusp tip deflection collected at 1 h, 24 h, and 7 days after light exposure, axial shrinkage strain and stress, recorded at 1 h and 24 h post irradiation and the flexural modulus (E) as provided by the manufacturers.

DISCUSSION

This work investigated the cusp deflection of standardized Al tooth models with a MOD cavity restored with three specially selected bulk-fill RBCs: A conventional bulk-fill RBC (Aura) using classical dimethacryclates such as Bis-GMA, TEGDMA, and UDMA , the second RBC (Filtek One) was made with stress-relieving AFM monomers in a nanofiller matrix, and the third RBC (Admira) consisted of a ORMOCER-based nanohybrid fillers in a resin matrix with nonclassical monomers. For comparison purposes, Filtek One was used as the control.

As no debonding occurred along the cavity walls that had been treated with the primer, with or without the adhesive, the bond strength anywhere along the interfaces in these samples was greater than the local shrinkage stress. As a result, the cusp tip deflections depended only on the RBC's shrinkage characteristics, the configuration factor (C-factor) —or more precisely the stiffness of the cavity wall relative to that of the cured RBC— and the operator-related restoration reproducibility[11,57].

The cusp tip deflections measured for the 3 groups of samples at 1 h, 24 h, and 7 days after light exposure are summarized in Fig. 5. The statistical analysis indicated that, for each of the three post-irradiation times, the mean cusp tip deflection of tooth models restored using Aura and Filtek One were not significantly different (α=0.05), while they were significantly greater than that of Admira. Consequently, the first null hypothesis that the differences in the mean cusp tip deflection among the three RBCs are not statistically significant is partially rejected.

Although the statistical power for the shrinkage strain and stress data shown in Fig. 6 is only 37.1%, the differences in strain and stress values within groups of three repeats is attributed to small differences in sample thickness used to collect the data. The coefficient of variation (ratio of the standard deviation to the average) of the strain and stress values within each group at 24 h was less than 2% and 6%, or in thickness variation of less than 20 μm and 60 μm, respectively.

The axial shrinkage strain (ε) and stress (S) data in Fig. 6 clearly show that, for all times, the smallest ε and S values were those for Admira, which were consistent with the cusp tip deflection data. The very low mean cusp tip deflection, axial shrinkage strain and shrinkage stress could be partly attributed to this RBC's nanohybrid composition that had a high 84 wt% (69 vol%) of filler and low resin content. Furthermore, its ORMOCER monomers occupy a much larger volume and has a much larger molecular weight than each of the classical monomer. On the other hand, its high flexural modulus of 10.1 GPa should lead to greater shrinkage stress and more cusp tip deflection. A possible reason for the unexpected result may be that the development of its stiffness, and hence shrinkage stress, lags behind the development of the shrinkage strain due, for instance, to delayed cross-linking. This tentative explanation is consistent with the results shown in Figs. 7 and 8 where there is a large time lag in development between shrinkage stress and shrinkage strain for Admira compared to the time lag observed for the other two RBCs.

The ε and S values for Filtek One were significantly smaller than those for Aura. The second null hypothesis that the differences in the mean values of ε and S among the three RBCs are not statistically significant is thus rejected. The smaller values of ε and S for Filtek One were tentatively attributed in part to its resin chemistry. One of its monomers consists of a high-molecular-weight aromatic urethane dimethacrylate (AUDMA) which decreases the number of reactive groups in the resin, resulting in a lower shrinkage strain. The second monomer, referred to as AFM[16], is designed to cleave through a fragmentation process during polymerization to lower shrinkage stress. A past study showed that the cusp tip deflection of Al tooth models decreased with increasing AFM content in the RBC[43]. Interestingly, despite the lower values of ε and S for Filtek One compared to those for Aura, the mean cusp tip deflections for these two RBCs did not differ significantly. These results appear contradictory. The tensometer used for measuring the axial shrinkage stress was compliant (a=0.20 μm/N) and, as a result, the shrinkage stress was dictated mainly by the shrinkage strain[58,59] with the consequence that the ordering of the shrinkage stress being the same as that of the shrinkage strain between Filtek One and Aura. On the other hand, while the Al tooth model has a compliance of approximately 0.17 μm/N at the cusp tip, the compliance decreases to approximately zero at the cavity floor. As a result, the RBC stiffness becomes an important factor when determining the cusp tip deflection[57]. The flexural modulus of Aura of 8.7±0.2 GPa was much lower than that of Filtek One of 11.3±0.3 GPa. This additional factor may have resulted in similar cusp tip deflections for these two RBCs despite the very different shrinkage stress values given by the tensometer. Further study is required to elucidate this aspect.

To gain additional insight into the polymerization process of each RBC, it is interesting to study the time evolution of D, ε, and S for each RBC. The time evolution can be illustrated by comparing the mean values of D at 1 h relative to those at 24 h with the corresponding relative values for ε and S. The mean values of D at 1 h relative to those at 24 h were 88%, 84%, and 79% for Aura, Filtek One, and Admira, respectively. The corresponding values for ε and S, *i.e.* ε(1 h)/ε(24 h) and S(1 h)/S(24 h), were 91.2% and 90.7%, 87.6% and 87.5%, and 88.9% and 87.0% for Aura, Filtek One, and Admira, respectively. Note that for the three RBCs the ratios of ε(1 h)/ε(24 h) and S(1 h)/S(24 h) are similar because the shrinkage stress was driven mostly by the shrinkage strain due to the high compliance of the tensometer. While the relative mean values of D for Aura and Filtek One were comparable to those for ε and S, the relative mean values of D for Admira (79%) were appreciably lower than those for ε and S (87–89%). These results suggest that additional time was required for the stiffness of Admira to develop, which is consistent with the results shown in Fig. 8. This difference is attributed to the unique composition of Admira compared to the other two RBCs. For Aura and Admira, the mean value of D plateaued at a time between 1 h and 24 h. The mean value of D for Filtek One further increased by 7.4% from 24 h to 7 days.

As noted above, the mean cusp tip deflection at 7 days was significantly greater than that at 24 h for Filtek One, which was not observed for the other two RBCs. The increase in mean cusp tip deflection at 7 days for Filtek One may be due to the continued polymerization produced by the interaction between the persistent residual radicals and polymer network. Further work is required to evaluate the role of the AFM monomers in the development of shrinkage stress in Filtek One.

One day (or 7 days) after light exposure, the standard deviation for the cusp tip deflection was 0.80 μm (or 0.84 μm) and 0.58 μm (or 0.63 μm) for Aura and Admira, respectively, which were less than half of that for Filtek One [1.89 μm (or 1.90 μm)]. The large standard deviation for Filtek One's cusp tip deflection may be due to the role played by the AFM monomers and the prolonged presence of the residual radicals during the curing process. Unlike the shrinkage strain and stress measurements that used 1 mm thick samples, the tooth model restoration was 4 mm deep. The penetration depth of blue light in a bulk fill RBC is about 1.3 mm[60], more than the sample thickness of 1 mm for shrinkage stress and strain measurements, but much less than the 4 mm deep restoration. As a result, there will be a large decrease in photoexcitation and hence in photoinitiation across the restoration depth. In addition, there will also be a large decrease in compliance along the restoration depth, resulting in the AFM monomers being more active in the higher stress region near the cavity floor than near the cusp tip[11]. The AFM random distribution and action, similar to those of a photoinitiator in an RBC that can lead to heterogeneity in its shrinkage strain field[61], will likely add to the variation of the cusp tip deflection.

Figures 6 and 7 indicate that, 5 min after the start of photoexposure, the shrinkage strain and stress reached between 72% and 81%, and between 64% and 75% of their values at 24 h, respectively. They then reached 90% of their values at 24 h after 40–113 min and 51–118 min, respectively. A past study[31] also showed that the order of shrinkage stress of two RBCs switched 4.5 h after the start of photoexposure. All these results suggest that the shrinkage strain and stress should continue to be measured hours after light exposure.

The challenging problem of high shrinkage stress has been partially addressed by the manufacturers by implementing specially designed monomers to minimize the shrinkage strain and to relieve the associated shrinkage stress. The comparison between the mean cusp tip deflections among the three RBCs and the ratio between the normalized shrinkage stress and normalized shrinkage strain confirm that an alternative strategy to reduce shrinkage stress is *to delay* the development of the elastic modulus of the RBC relative to the shrinkage strain.

The findings of this work indicate that the cusp tip deflection of standardized Al tooth models is a much more clinically relevant measurement to evaluate the impact of the curing RBC on premolar or molar tooth restoration with a Class II MOD cavity than either the axial shrinkage strain or stress from simple disc specimens. The Al tooth model provides a range of compliance mimicking that in a human tooth with a Class II MOD cavity, instead of the fixed compliance of a tensometer. Because of this, the tooth model can aptly take into account the impact of the RBC stiffness and its time evolution on the cusp deflection or shrinkage stress. The simple rectangular shape of the model allowed very precise and accurate measurements of the cusp deflection up to 7 days after light exposure. In addition, debonding was prevented, thus making these findings independent of the bond strength or the microscopic mechanisms leading to its formation. The highly precise measurement enabled the impact of the RBCs' polymerization kinetics on the cusp deflection to be assessed comprehensively.

CONCLUSIONS

Within the limitations of this *in vitro* study, it was concluded that:

1. The mean cusp tip deflection of restored aluminium tooth models with standardized dimensions and alloy type is a much more clinically relevant measurement than data obtained using either the axial shrinkage strain or stress techniques. The Al tooth model mimics the compliance of human teeth with MOD cavity. As a result, not only the shrinkage strain and its rate of development of an RBC play a role in the cusp tip deflection but also the development of its stiffness relative to its strain with time.
2. Although Filtek One bulk-fill produced a lower shrinkage strain and stress than Aura Bulk-fill, the mean cusp tip deflections of these two RBCs

were not significantly different, indicating the complex interaction of material properties in determining clinical outcomes.

3. Admira Fusion x-tra universal shade exhibited the smallest mean cusp tip deflection up to 7 days post-curing. This was attributed to its unique ORMOCER-nanohybrid filler composition, which caused minimal shrinkage strain and delayed development of stiffness relative to shrinkage strain.

ACKNOWLEDGMENTS

This work was supported in part by the authors' institution. We would like to thank J. Dahn for the use of his profilometer. We are very grateful to B. VanHeel at the Minnesota Dental Research Center for Biomaterials and Biomechanics (MDRCBB) for performing the micro-CT measurements and image reconstructions. We would like to thank J. Stansbury, University of Colorado School of Dental Medicine; J. Oxman; A. Fok, MDRCBB and M. Mehring, Voco, Cuxhaven, Germany for fruitful discussions. We are grateful to 3M Oral Care for the donation of the LCU, adhesive, and RBC, Ivoclar Vivadent for the donation of the primer, VOCO, and SDI for the donation of the RBCs used in this study. We would also like to thank P. Farrar SDI and G. Connell VOCO for providing us their RBC flexural modulus.

CONFLICT OF INTEREST

The authors declare no conflicts of interest associated with this manuscript.

REFERENCES

1) Oliveira LRS, Braga SSL, Bicalho AA, Ribeiro MTH, Price RB, Soares CJ. Molar cusp deformation evaluated by micro-CT and enamel crack formation to compare incremental and bulk-filling techniques. J Dent 2018; 74: 71-78.
2) Behery H, El-Mowafy O, El-Badrawy W, Saleh B, Nabih S. Cuspal deflection of premolars restored with bulk-fill composite resins. J Esthet Restor Dent 2016; 28: 122-130.
3) Bicalho AA, de Souza SJ, de Rosatto CM, Tantbirojn D, Versluis A, Soares CJ. Effect of temperature and humidity on post-gel shrinkage, cusp deformation, bond strength and shrinkage stress —Construction of a chamber to simulate the oral environment. Dent Mater 2015; 31: 1523-1532.
4) Güler E, Karaman E. Cuspal deflection and microleakage in pre molar teeth restored with bulk-fill resin-based composites. J Adhes Sci Technol 2014; 28: 2089-2099.
5) Moorthy A, Hogg CH, Dowling AH, Grufferty BF, Benetti AR, Fleming GJ. Cuspal deflection and microleakage in premolar teeth restored with bulk-fill flowable resin-based composite base materials. J Dent 2012; 40: 500-505.
6) da Silva Pereira RA, de Braganca GF, Vilela A, de Deus RA, Miranda RR, Verissimo C, *et al*. Post-gel and total shrinkage stress of conventional and bulk-fill resin composites in endodontically-treated molars. Oper Dent 2020; 45: E217-E226.
7) Yarmohamadi E, Jahromi PR, Akbarzadeh M. Comparison of cuspal deflection and microleakage of premolar teeth restored with three restorative materials. J Contemp Dent Pract 2018; 19: 684-689.
8) Ferracane JL, Hilton TJ. Polymerization stress —Is it clinically meaningful? Dent Mater 2016; 32: 1-10.
9) Gallo M, Abouelleil H, Chenal JM, Adrien J, Lachambre J, Colon P, *et al*. Polymerization shrinkage of resin-based composites for dental restorations: A digital volume correlation study. Dent Mater 2019; 35: 1654-1664.
10) Tsujimoto A, Jurado CA, Barkmeier WW, Sayed ME, Takamizawa T, Latta MA, *et al*. Effect of layering techniques on polymerization shrinkage stress of high- and low-viscosity bulk-fill resins. Oper Dent 2020; 45: 655-663.
11) Pottier JG, Gregg A, Aregawi W, Nasiri E, Fok A, Liu Y, *et al*. A standardized method to determine the effect of polymerization shrinkage on the cusp deflection and shrinkage induced built-in stress of class II tooth models. J Mech Behav Biomed Mater 2020; 111: 103987.
12) Magne P, Oganesyan T. Premolar cuspal flexure as a function of restorative material and occlusal contact location. Quintessence Int 2009; 40: 363-370.
13) Yazici AR, Kutuk ZB, Ergin E, Karahan S, Antonson SA. Six-year clinical evaluation of bulk-fill and nanofill resin composite restorations. Clin Oral Investig 2022; 26: 417-426.
14) Schoilew K, Fazeli S, Felten A, Sekundo C, Wolff D, Frese C. Clinical evaluation of bulk-fill and universal nanocomposites in class II cavities: Five-year results of a randomized clinical split-mouth trial. J Dent 2023; 128: 104362.
15) Cho K, Rajan G, Farrar P, Prentice L, Prusty BG. Dental resin composites: A review on materials to product realizations. Compos B Eng 2022; 230: 109495.
16) Shah PK, Stansbury JW, Bowman CN. Application of an addition-fragmentation-chain transfer monomer in di(meth) acrylate network formation to reduce polymerization shrinkage stress. Polym Chem 2017; 8: 4339-4351.
17) AlSahafi R, Wang X, Mitwalli H, Alhussein A, Balhaddad AA, Melo MAS, *et al*. Novel antibacterial low-shrinkage-stress resin-based cement. Dent Mater 2022; 38: 1689-1702.
18) Fugolin AP, Lewis S, Logan MG, Ferracane JL, Pfeifer CS. Methacrylamide-methacrylate hybrid monomers for dental applications. Dent Mater 2020; 36: 1028-1037.
19) Lewis SH, Fugolin APP, Bartolome A, Pfeifer CS. Relaxation mechanisms in low-stress polymer networks with alternative chemistries. JADA Found Sci 2024; 3: 100033.
20) Graff B, Klee JE, Fik C, Maier M, Fouassier JP, Lalevee J. Development of novel photoinitiators as substitutes of camphorquinone for the LED induced polymerization of methacrylates: A bis-silyl ketone. Macromol Rapid Commun 2017; 38: 1600470.
21) Moszner N, Fischer UK, Ganster B, Liska R, Rheinberger V. Benzoyl germanium derivatives as novel visible light photoinitiators for dental materials. Dent Mater 2008; 24: 901-907.
22) Kowalska A, Sokolowski J, Bociong K. The photoinitiators used in resin based dental composite —A review and future perspectives. Polymers (Basel) 2021; 13: 470.
23) Delgado AJ, Castellanos EM, Sinhoreti M, Oliveira DC, Abdulhameed N, Geraldeli S, *et al*. The use of different photoinitiator systems in photopolymerizing resin cements through ceramic veneers. Oper Dent 2019; 44: 396-404.
24) Randolph LD, Palin WM, Bebelman S, Devaux J, Gallez B, Leloup G, *et al*. Ultra-fast light-curing resin composite with increased conversion and reduced monomer elution. Dent Mater 2014; 30: 594-604.
25) Ionescu AC, Comba A, Brambilla E, Ilie N, Breschi L, Cadenaro M, *et al*. Influence of curing time on the microbiological behavior of bulk-fill nanohybrid resin composites. Polymers (Basel) 2021; 13: 2948.
26) Elfakhri F, Alkahtani R, Li C, Khaliq J. Influence of filler characteristics on the performance of dental composites: A comprehensive review. Ceram Int 2022; 48: 27280-27294.
27) Wang R, Habib E, Zhu XX. Evaluation of the filler packing

structures in dental resin composites: From theory to practice. Dent Mater 2018; 34: 1014-1023.
28) Kundie F, Azhari CH, Muchtar A, Ahmad ZA. Effects of filler size on the mechanical properties of polymer-filled dental composites: A review of recent developments. J Phys Sci 2018; 29: 141-165.
29) Elbishari H, Silikas N, Satterthwaite J. Filler size of resin-composites, percentage of voids and fracture toughness: Is there a correlation? Dent Mater J 2012; 31: 523-527.
30) Germscheid W, de Gorre LG, Sullivan B, O'Neill C, Price RB, Labrie D. Post-curing in dental resin-based composites. Dent Mater 2018; 34: 1367-1377.
31) Kalliecharan D, Germscheid W, Price RB, Stansbury J, Labrie D. Shrinkage stress kinetics of bulk fill resin-based composites at tooth temperature and long time. Dent Mater 2016; 32: 1322-1331.
32) Van Ende A, De Munck J, Lise DP, Van Meerbeek B. Bulk-fill composites: A review of the current literature. J Adhes Dent 2017; 19: 95-109.
33) Leprince JG, Palin WM, Vanacker J, Sabbagh J, Devaux J, Leloup G. Physico-mechanical characteristics of commercially available bulk-fill composites. J Dent 2014; 42: 993-1000.
34) Soares CJ, Rosatto C, Carvalho VF, Bicalho AA, Henriques J, Faria ESAL. Radiopacity and porosity of bulk-fill and conventional composite posterior restorations —Digital X-ray analysis. Oper Dent 2017; 42: 616-625.
35) Jarisch J, Lien W, Guevara PH, Greenwood WJ, Dunn WJ. Microcomputed tomographic comparison of posterior composite resin restorative techniques: Sonicated bulk fill versus incremental fill. Gen Dent 2016; 64: 20-23.
36) Enochs T, Hill AE, Worley CE, Verissimo C, Tantbirojn D, Versluis A. Cuspal flexure of composite-restored typodont teeth and correlation with polymerization shrinkage values. Dent Mater 2018; 34: 152-160.
37) Kim YJ, Kim R, Ferracane JL, Lee IB. Influence of the compliance and layering method on the wall deflection of simulated cavities in bulk-fill composite restoration. Oper Dent 2016; 41: e183-e194.
38) Tsujimoto A, Nagura Y, Barkmeier WW, Watanabe H, Johnson WW, Takamizawa T, *et al*. Simulated cuspal deflection and flexural properties of high viscosity bulk-fill and conventional resin composites. J Mech Behav Biomed Mater 2018; 87: 111-118.
39) Chun K, Choi H, Lee J. Comparison of mechanical property and role between enamel and dentin in the human teeth. J Dent Biomech 2014; 5: 1758736014520809.
40) Suiter EA, Watson LE, Tantbirojn D, Lou JS, Versluis A. Effective expansion: Balance between shrinkage and hygroscopic expansion. J Dent Res 2016; 95: 543-549.
41) Taylor R, Fuentealba R, Brackett WW, Roberts HW. 24 hour polymerization shrinkage of resin composite core materials. J Esthet Restor Dent 2021; 33: 775-785.
42) Kaiser C, Price RB. Effect of time on the post-irradiation curing of six resin-based composites. Dent Mater 2020; 36: 1019-1027.
43) Falsafi A, Oxman JD, Tse PH, Ton TT. Longer-term postcure measurement of cuspal deformation induced by dimensional changes in dental materials. Int J Dent 2015; 2015: 915071.
44) Barceleiro MdO, Tardem C, Albuquerque EG, Lopes LdS, Marins SS, Poubel LA, *et al*. Can composite packaging and selective enamel etching affect the clinical behavior of bulk-fill composite resin in posterior restorations? 24-month results of a randomized clinical trial. J Appl Oral Sci 2023; 31: e20220323.
45) Cieplik F, Hiller K-A, Buchalla W, Federlin M, Scholz KJ. Randomized clinical split-mouth study on a novel self-adhesive bulk-fill restorative vs. a conventional bulk-fill composite for restoration of class II cavities–results after three years. J Dent 2022; 125: 104275.
46) Szebeni D, Told R, Kunsági-Máté S, Szalma J, Maróti P, Böddi K, *et al*. Monomer elution and shrinkage stress analysis of addition-fragmentation chain-transfer-modified resin composites in relation to the curing protocol. Dent Mater 2024; 40: 1611-1623.
47) de Deus R, Oliveira L, Braga S, Ribeiro M, Price R, Núñez A, *et al*. Effect of radiant exposure on the physical and mechanical properties of 10 flowable and high-viscosity bulk-fill resin composites. Oper Dent 2024; 49: 136-156.
48) Ribeiro MTH, de Bragança GF, Oliveira LRS, Braga SSL, de Oliveira HLQ, Price RB, *et al*. Effect of pre-heating methods and devices on the mechanical properties, post-gel shrinkage, and shrinkage stress of bulk-fill materials. J Mech Behav Biomed Mater 2023; 138: 105605.
49) O'Neill C, Kreplak L, Rueggeberg FA, Labrie D, Shimokawa CAK, Price RB. Effect of tooth brushing on gloss retention and surface roughness of five bulk-fill resin composites. J Esthet Restor Dent 2018; 30: 59-69.
50) Price RB, Rueggeberg FA, Labrie D, Felix CM. Irradiance uniformity and distribution from dental light curing units. J Esthet Restor Dent 2010; 22: 86-101.
51) Price RB, Labrie D, Rueggeberg FA, Felix CM. Irradiance differences in the violet (405 nm) and blue (460 nm) spectral ranges among dental light-curing units. J Esthet Restor Dent 2010; 22: 363-377.
52) Carrera CA, Lan C, Escobar-Sanabria D, Li Y, Rudney J, Aparicio C, *et al*. The use of micro-CT with image segmentation to quantify leakage in dental restorations. Dent Mater 2015; 31: 382-390.
53) Kostylev I, Labrie D, Price RBT. Time-resolved 2D shrinkage field of dental resins using laser interferometry. Appl Opt 2015; 54: 1852-1860.
54) Kostylev I, Winters T, Labrie D, Price RB. Role of the beam profile and sample geometry in the bonded-disk method on the shrinkage kinetics of two dental resins. Dent Mater 2016; 32: 1026-1035.
55) Faul F, Erdfelder E, Lang A-G, Buchner A. G* Power 3: A flexible statistical power analysis program for the social, behavioral, and biomedical sciences. Behav Res Methods 2007; 39: 175-191.
56) Faul F, Erdfelder E, Buchner A, Lang A-G. Statistical power analyses using G* Power 3.1: Tests for correlation and regression analyses. Behav Res Methods 2009; 41: 1149-1160.
57) Aregawi WA, Fok ASL. Shrinkage stress and cuspal deflection in MOD restorations: Analytical solutions and design guidelines. Dent Mater 2021; 37: 783-795.
58) Fok AS. Shrinkage stress development in dental composites —An analytical treatment. Dent Mater 2013; 29: 1108-1115.
59) Aregawi WA, Fok ASL. 1/(2+R(c)): A simple predictive formula for laboratory shrinkage-stress measurement. Dent Mater 2017; 33: 536-542.
60) Labrie D, Price RB, Sullivan B, Salazar AM, Gautam D, Stansbury JW, *et al*. Effect of thickness on the degree of conversion of two bulk-fill and one conventional posterior resin-based composites at high irradiance and high temporal resolution. J Mech Behav Biomed Mater 2022; 136: 105489.
61) Li J, Fok AS, Satterthwaite J, Watts DC. Measurement of the full-field polymerization shrinkage and depth of cure of dental composites using digital image correlation. Dent Mater 2009; 25: 582-588.